Electronic Supplementary Material (ESI) for Chemical Communications.

Supporting Information for: Cation Coordination Polyhedra Lead to Multiple Lengthscale Organization in Aqueous Electrolytes

Yihui Wei,*,† Emily T. Nienhuis,*,‡ Sebastian T. Mergelsberg,‡ Trent R. Graham,† Qing Guo,† Gregory K. Schenter,‡ Carolyn I. Pearce,‡,¶ and Aurora E. Clark*,†,‡

†*Department of Chemistry, University of Utah, Salt Lake City, UT, USA*

‡*Pacific Northwest National Laboratory, Richland, WA, USA*

¶*Department of Crop and Soil Sciences, Washington State University, Pullman, WA, USA*

E-mail: yihui.wei@utah.edu; emily.nienhuis@pnnl.gov; aurora.clark@utah.edu

Sample Preparation & Experimental Methodology

Samples for this study were prepared by dissolving either $NaNO_2$ (Sigma Aldrich, >99.0%) or $NaNO_3$ (Sigma Aldrich, >99.0%) into DDI water (miliQ, 18.2 MΩ·cm) to produce 10 m (molal, moles solute per kilogram solvent) stock solutions. Dissolution of the salt was facilitated by magnetic stirring with a Teflon-coated magnetic stir bar. Solutions were prepared under N_2 (g) in a glovebox to prevent uptake of CO_2 (g) and due to the hygroscopic nature of the nitrate and nitrite reagent salts. To prepare the other concentrations used in this study, aliquots of known masses from the 10 m stock solutions were then diluted by mass with DDI water (miliQ, 18.2 MΩ·cm). To prepare the sample denoted 'concentrated,' either

$NaNO_2$ or $NaNO_3$ was added to DDI water, while stirring with a magnetic stir bar, until there was residual, undissolved salt remaining in the solution. These solutions were continuously stirred for 24 hours to allow for further dissolution of the salt prior to collection of the supernatant. The supernatant from the concentrated solutions was collected and filtered through a 0.45 μm syringe filter to remove any undissolved solid, which would otherwise interfere with the X-ray total scattering measurement. Solutions were loaded into 1.9 mm OD polyimide (Kapton) capillaries that were approximately 1.5 inches in length.

Capillaries containing the $NaNO_2$ and $NaNO_3$ solutions were loaded into the automatic sample shifter at beamline 11-ID-B of the Advanced Photon Source to obtain X-ray total scattering data for pair distribution function, PDF, analysis. The incident X-ray beam energy was 86.7 keV (0.1432 Å), which was aligned with the capillaries containing the nitrate and nitrite solutions as to maximize the detected signal (i.e. the X-ray beam was aligned with the largest diameter of the sample). Scattered X-rays were detected on a Perkin Elmer amorphous silicon flat plate detector with dimensions of 2048 x 2048 pixels and 200 μm x μm pixels. The detector angle, tilt angle, and the detector distance were calibrated using a crystalline CeO_2 standard diluted to 1:20 with glassy carbon. Prior to measurement of each sample, a dark image of the detector was obtained. Samples were measured with 0.5 second exposure and 720 exposures per image. Eight images were summed together for each sample. An empty capillary was also measured under the same conditions to account for air and capillary scattering to be used in the background subtraction in the data processing discussed in the subsequent steps.

GSAS-II was used to perform the detector calibration and to integrate the 2D detector images to the 1D intensity data, $I(Q)$ and $I(2\theta)$.[1] GSAS-II was additionally used to mask the beamstop as well as any 'dead' or 'hot' pixels that would negatively impact the 2D to 1D data transformation.

PDFgetX2 was used to process the intensity data to the $F(Q)$, $S(Q)$, and the $G(r)$.[2] $G(r)$ in the context of this study is referred to as the pair distribution function, or PDF.

The empty capillary background was subtracted from the intensity data of all samples. The atomic composition was assumed to be that of the as-prepared solutions, including the water content. The Q-min and Q-max for the Fourier Transformation were set to 0.5 $Å^{-1}$ and 24 $Å^{-1}$, respectively. Q-max was determined based upon where data where noise was minimal, but relevant structural information was still available. The resulting $F(Q)$ and $S(Q)$ were output as 0.5-24.0 $Å^{-1}$, and the $G(r)$ was output with a range of 0.0-16.0 Å, with a step size of 0.1 Å. For an example of general parameters used in PDFgetX2, see the file: PDFgetX2-processing-example.gr provided in the Supplementary Information.

Computational Methodology

Molecular Dynamics Protocol. Classical molecular dynamics simulations were performed using GROMACS[3] with initial configurations based upon concentration dependent experimental densities and created in PACKMOL.[4] Table S1 presents the molecular compositions of each simulation periodic cubic box. Initial equilibration of each system consisted of 5 ns of NVT at 350 K, followed by 5 ns of NPT ensemble equilibration at 300 K, 1 bar and another 5 ns NVT equilibration step at 300 K. Production runs for data analysis were collected at 300 K at NVT ensemble for 40 ns. The Nose-Hoover thermostat[5,6] was used for temperature coupling and Parrinelo-Rahman barostat[7] for pressure coupling. The Van der Waals and short-range electrostatic interactions employed a real-space cutoff of 0.9 nm. The particle Mesh Ewald (PME) summation method[8] was employed to compute the long-range electrostatic energy. For each system the SPC water model,[9] where the LINCS algorithm[10] was used to constraint intramolecular O-H bonds in water molecules. Interatomic interactions for Na^+ were based on the GROMOS 53A6 force field.[11] The potentials for NO_2^- and NO_3^- interactions were developed by Cordeiro *et al.*.[12] This force field combination was validated against the experimental X-ray pair distributions as a function of electrolyte concentration, as described below. A geometric average combination rule was used for generating Lennard-Jones

pairwise interactions. CMD trajectories are used to generate simulated PDFs weighted by X-ray scattering length and non-X-ray Radial Distribution Functions (RDFs) that describes atomic pair-wise correlations.

Table S1: Molecular compositions and simulation box parameters employed within the classical MD simulations of $NaNO_{3(aq)}$ and $NaNO_{2(aq)}$.

$NaNO_2$ concentration (m)	1.1	1.9	2.4	2.9	3.8
Number of $NaNO_2$ per box	22	30	37	45	65
Number of H_2O per box	1097	900	870	860	945
Equilibrium volume (nm^3)	34.06	28.22	27.62	27.64	30.53

$NaNO_2$ concentration (m)	6	7	9.3	10.5	13
Number of $NaNO_2$ per box	87	100	120	120	153
Number of H_2O per box	805	790	720	633	655
Equilibrium volume (nm^3)	27.34	27.74	26.81	24.11	26.78

$NaNO_3$ concentration (m)	1	2.8	5.2	8.5	10.4	13
Number of $NaNO_3$ per box	39	45	70	92	94	153
Number of H_2O per box	2169	898	750	601	500	655
Equilibrium volume (nm^3)	68.61	29.93	27.01	23.8	20.94	29.14

Force Field Validation and Benchmarking. Several force field combinations were examined for their ability to reproduce the concentration dependent experimental X-ray pair distribution functions of $NaNO_{3(aq)}$ and $NaNO_{2(aq)}$. The X-ray total pair distribution function, $G(r)$, is defined as the combination of all atomic pair distribution functions in the system.

$$G(r) = \sum_{i,j=1}^{n} c_i c_j \bar{b_i} \bar{b_j} [g_{ij}(r) - 1] \tag{S1}$$

where c_i is the concentration of particle i and $\bar{b_i}$ is the coherent scattering length of particle i. In order for a direct comparison between the experimentally obtained PDF and that obtained from the classical molecular dynamics simulations, DISCUS was employed.[13] DISCUS uses the classical molecular dynamics trajectory files as the input, as well as the configuration from the X-ray total scattering experiment, to produce a simulated PDF with the same nor-

Table S2: Final validated force field parameters for $NaNO_{3(aq)}$ and $NaNO_{2(aq)}$ employed in this study from Ref. 12.

Interaction type	σ (nm)	ϵ (kJ/mol)	Charge (e)
Na	0.258	0.062	1
O_W	0.317	0.65	-0.82
Hw	0	0	0.41
N in NO_3	0.334	0.438	0.65
O in NO_3	0.263	1.725	-0.55
N in NO_2	0.334	0.438	0.4
O in NO_2	0.263	1.725	-0.7

malization scheme. In practice, it has been noticed in many systems[14–16] that the intensities of simulated PDF from DISCUS and experiment PDF from PDFgetX2 may differentiate by a scalar of a multiple of π. In order to have a direct comparison, we manually multiplied the simulated intensities $G(r)$ with π. Broadening and dampening factors could be initiated in DISCUS to reproduce the similar Fourier broadening and dampening and termination ripples when transforming from Q-space to real space as experimental $G(r)$. For the purpose of precisely determining the peak positions, we disabled these factors for all simulated $G(r)$ displayed in this paper.

The ability to reproduce the experimental PDFs across the experimental concentration range has been investigated for different $NaNO_{3(aq)}$ and $NaNO_{2(aq)}$ force fields as shown in Figure S1. Four $NaNO_3$ force fields that have been tested here were reported by Cordeiro et. al.,[12] Megyes et al.,[17] Wipff et al.[18] and Zou et al.[19] Three different models representating NO_3^- were similarly tested; these are the potentials of Cordeiro et. al.,[12] Kam et al.[20] and Richards et al.[21] Table S3 presents the water and ion models for those force fields that have been examined the physicochemical and structural properties of these solutions under a range of different concentrations by prior literature.

Figure S1 compares the simulated total XRD PDF for different force fields to the experimental PDF. For both $NaNO_3$ and $NaNO_2$, at shorter distances (from 1 Å to 5 Å), the

Table S3: Different force fields tested for $NaNO_3$ and $NaNO_2$ solutions.

Force fields	Water model	Ion model	Literature concentration.
Cordeiro $NaNO_3$[12] Cordeiro $NaNO_2$[12]	SPC[9]	GROMOS 53A6[11]	dilute, 1 M, 4.4 M dilute, 4.7 M
Megyes $NaNO_3$[17]	SPC/E[22]	OPLS all-atom[23]	1.9 M, 2.5 M, 5.6 M, 7.5 M
Wipff $NaNO_3$[18]	TIP3P[24]	OPLS all-atom	dilute
Zou $NaNO_3$[19]	SPC/E	Kirkwood-Buff force field	1 m, 3 m, 5 m
Kam $NaNO_2$[20]	TIP3P, SPC/E	Na^+: CHARMM[25] NO_2^-: Amber[26]	dilute
Richards $NaNO_2$[21]	TIP3P	Na^+: Joung-Cheatham[27] NO_2^-: By ab-initio techniques	dilute

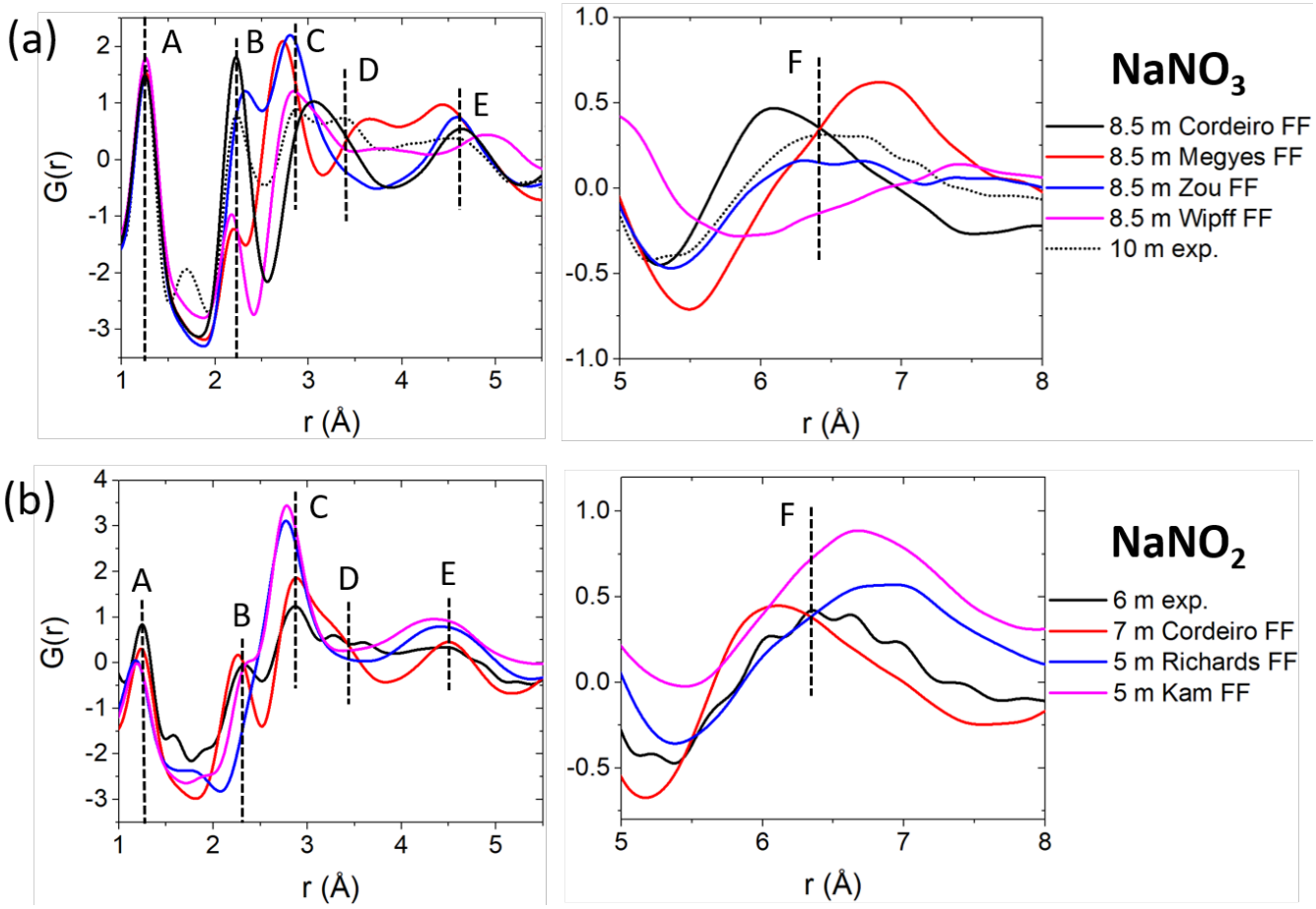

Figure S1: (a) Simulated and experimental X-ray PDF with different $NaNO_3$ force fields at shorter- and longer-range; (b) Simulated and experimental X-ray PDF with different $NaNO_3$ force fields at shorter- and longer-range. Cordeiro FF is used from Ref. 12.

Cordeiro force field shows better agreements for peak **A**, **B**, **E** and a combination of peak **C** and **D**. At longer distances (from 5 Å to 8 Å), the Cordeiro $NaNO_3$ parameters shows a structure feature at roughly 0.5 Å shorter than experimental peak **F** while the force field employed by Megyes for $NaNO_3$ has a feature 0.5 Å longer than experiment. For $NaNO_2$, the Cordeiro force field also produces a shorter structure feature while the rest of benchmarked force field show a longer structure feature with inconsistent trends as a function of electrolyte concentration. As the Cordeiro force field reproduces the trends of long-range peak feature observed in in Figures 2 and S1, it has been chosen for all concentrations discussed in the main text. As shown in Figures S2, at dilute conditions the average $Na\cdots O_W$ coordination number is 5.5, while the number of surrounding O_W about NO_3^- is 10.3 with a cutoff distance of 4.46 Å and about NO_2^- is 11.6 with a cutoff distance of 4.48 Å. These are in good agreement with prior reports of Ref. 28,29.

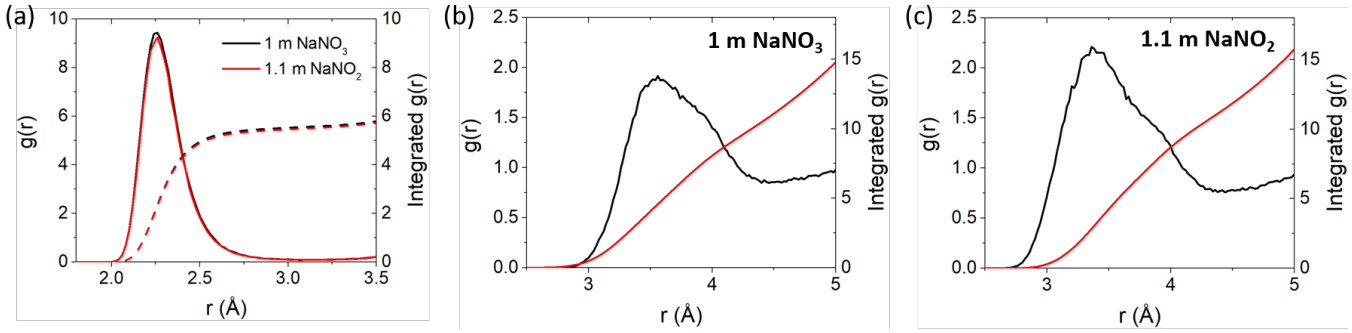

Figure S2: (a) Simulated $Na\cdots O_W$ RDF and integrated RDF plots at 1 m $NaNO_3$ and 1.1 m $NaNO_2$ using Cordeiro force field; (b) Simulated $N\cdots O_W$ RDF and integrated RDF plots at 1 m $NaNO_3$ using Cordeiro force field; (c) Simulated $N\cdots O_W$ RDF and integrated RDF plots at 1.1 m $NaNO_2$ using Cordeiro force field.

Ab initio Molecular Dynamics. Ab initio molecular dynamics (AIMD) simulations combined with the umbrella sampling (US) method are performed with Vienna Ab initio Simulation Package (VASP) code[30,31] to get the potential of mean force (PMF) of transformation between monodentate and bidentate for nitrate (NO_3^-) or nitrite (NO_2^-) with Na ion in water solution. The generalized gradient approximation (GGA) in the formulation of Perdew-Burke-Ernzerhof (PBE)[32] along with the projector augmented wave (PAW) method[33] was

used for the DFT simulations. The energy cutoff for the plane wave basis sets is set to 400 eV.

To simulate the solution phase, a 12 Å x 12 Å x 12 Å cubic simulation box containing 56 H_2O molecules and a nitrate-Na or a nitrite-Na pair is built with the Packmol code[4]. Only the gamma point is used for the Brillouin-zone sampling. In the AIMD simulations, tritium was used instead of hydrogen to permit a larger time step. Nosé-Hoover thermostat[5,6] is applied for the NVT simulations with a time step of 1 fs at 300 K. To implement the umbrella sampling simulations, the coordination number (CN) of Na with oxygen (O_N) in nitrate (NO_3^-) or nitrite (NO_2^-) is used as collective variables (CV) with the following formula:

$$CN = \sum_{i=1}^{M} \frac{1-(q_i/c_i)^n}{1-(q_i/c_i)^m}. \tag{S2}$$

Where i is the index of Na$\cdots$O$_N$ pairs, q_i is the distance of the i^{th} Na$\cdots$O$_N$ pair, and c_i is the reference distance which is 2.90 Å for Na$\cdots$O$_N$ here, and $n = 9$ and $m = 14$ using the default value within the VASP code.

In the US simulations, the CV values are constrained by a harmonic potential with a constant of 140 kcal/mol in seven individual windows from 0.8 to 2.0 with an interval of 0.2 in both cases of nitrate and nitrite. In each window, the system is equilibrated for 10 ps first, and another 10 ps is performed as the production run. Only the last 8 ps data are used to reconstruct the PMF with the WHAM code[34].

Simulation Analysis

Radial Distribution Functions

For the sake of simplicity, two different definitions of the radial distribution function were employed. For atom-pair correlations, the traditional RDF was calculated using

$$g_{ij}(r) = \frac{n_{ij}(r)}{4\pi r^2\, dr\, \rho_j}, \tag{S3}$$

where $n_{ij}(r)$ is the number of particles j between distance r and $r+dr$ away from a reference particle i and ρ_j is the bulk density for particle j.

In the case of groups of atoms pairs, for example all O-atoms within the network of Na^+ coordination polyhedra, a simplified definition - called the *partial* RDF $g^*(r)$ and XRD PDF $G^*(r)$ were employed. This is

$$G^*(r) = \frac{c_i c_j b_i b_j}{\left(\sum_i c_i b_i\right)^2} g^*(r) \tag{S4}$$

Chemical Networks of Intermolecular Interactions

Graphs of intermolecular interactions were employed to identify: 1) the ensemble distribution of local coordination environments to Na^+ including the composition, polyhedral geometry, and any oligomerization; 2) different H_2O and their hydrogen bonding patterns outside of any interactions to the electrolyte ions. To form a solution network graph, each molecule or ion in the solution is converted into a node and the intermolecular interactions are converted into edges using the geometric criteria in Table S4. Four types of inter-molecular edge interactions are identified: hydrogen bonds between H_2O ($O_W\cdots Hw$), hydrogen bonds between H_2O and polyoxo anions ($O_N\cdots Hw$), ion-pairing between Na^+ and polyoxo anions ($O_N\cdots Na$) and cation solvation by H_2O ($O_W\cdots Na$). The upper bounds for those edges vary from concentration to concentration, depending on the first minimum value indicated by atom-

pair RDF.

Table S4: Edge geometric criteria used to construct networks of intermolecular interactions within $NaNO_{3(aq)}$ and $NaNO_{2(aq)}$.The lower bounds for $O_N \cdots Hw$, $O_N \cdots Na$ and $O_W \cdots Na$ are 0 Å. The angle criteria for $O_W \cdots Hw$-O_W and $O_N \cdots Hw$-O_W are 150°-180° and 120°-180° respectively.

$NaNO_{2(aq)}$									
Concentration (m)	1.1	1.9	2.9	3.8	6	7	9.3	10.5	13
$O_W \cdots Hw$ lower bound (Å)	1.42	1.44	1.44	1.42	1.44	1.44	1.44	1.44	1.44
$O_W \cdots Hw$ upper bound (Å)	2.38	2.42	2.37	2.38	2.34	2.34	2.36	2.36	2.32
$O_N \cdots Hw$ upper bound (Å)	2.64	2.66	2.66	2.68	2.64	2.6	2.66	2.68	2.58
$O_N \cdots Na$ upper bound (Å)	3.02	3.22	3.14	3.16	3.1	3.24	3.14	3.18	3.26
$O_W \cdots Na$ upper bound (Å)	3.08	3.14	3.1	3.12	3.1	3.06	3.04	3.04	2.92

$NaNO_{3(aq)}$						
Concentration (m)	1	2.8	5.2	8.5	10.4	13
$O_W \cdots Hw$ lower bound (Å)	1.42	1.42	1.42	1.42	1.42	1.42
$O_W \cdots Hw$ upper bound (Å)	2.43	2.43	2.43	2.43	2.43	2.43
$O_N \cdots Hw$ upper bound (Å)	2.7	2.64	2.62	2.58	2.62	2.54
$O_N \cdots Na$ upper bound (Å)	3.14	3.1	3.16	3.2	3.22	3.32
$O_W \cdots Na$ upper bound (Å)	3.06	3.1	3.08	3.12	3.14	3.14

Polyhedron and Connected polyhedron Analysis

The goal of this work was to identify all coordination environments about the Na^+ and the polyhedral coordination environment involving the O-atoms of water and nitrate or nitrite anions. Toward this end, we first identified all subgraphs of the intermolecular network that had the Na^+ as the central node and its nearest neighbor connected vertices. Then, using method described in Ref. 35 we identified geometric edge criterion between the vertices of the coordination polyhedron and created a stochastic adjacency matrix of the subgraph; this was then employed in the equation for PageRank[36] and the leading eigenvector with eigenvalue 1 has entries for each node that are its PageRank value. To identify the connected polyhedra, we compared the coordinating O-atom indices for every vertex of the polyhedron. If two polyhedra are sharing a single oxygen atom, they would be identified as corner-sharing, edge-sharing if they are connected through two common oxygen atoms and face-sharing if

sharing three O-atoms.

With the identification of coordination polyhedra about Na^+, O-atoms from H_2O and the oxyanions could be separated into two classes, those coordinating Na^+ and those not. Those O-atoms coordinating Na^+ are labelled as being part of the network of Na^+-centered coordination polyhedra. Any H_2O not coordinating the Na^+ are considered part of the "bulk water" state. This is illustrated in Figure S11 (b). Although one may think that the H_2O solvating the oxyanion may have perturbed $O_W \cdots O_W$ correlations, the H_2O in the loose anion coordination shells have the same correlations as bulk water.

Results

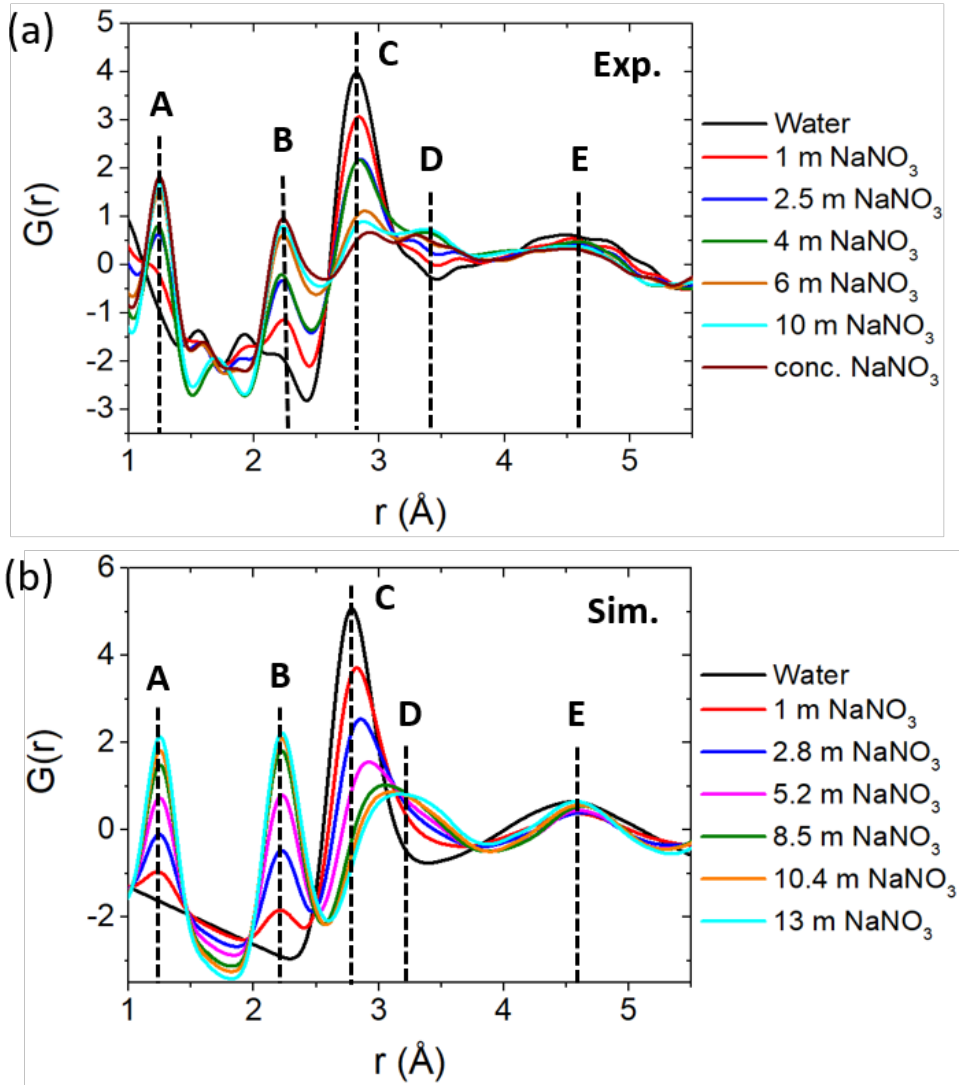

Figure S3: Short- and mid-range experimental (a) and simulated (b) total X-ray PDFs for $NaNO_{3(aq)}$. Simulated $G(r)$ is calculated using DISCUS.[13]

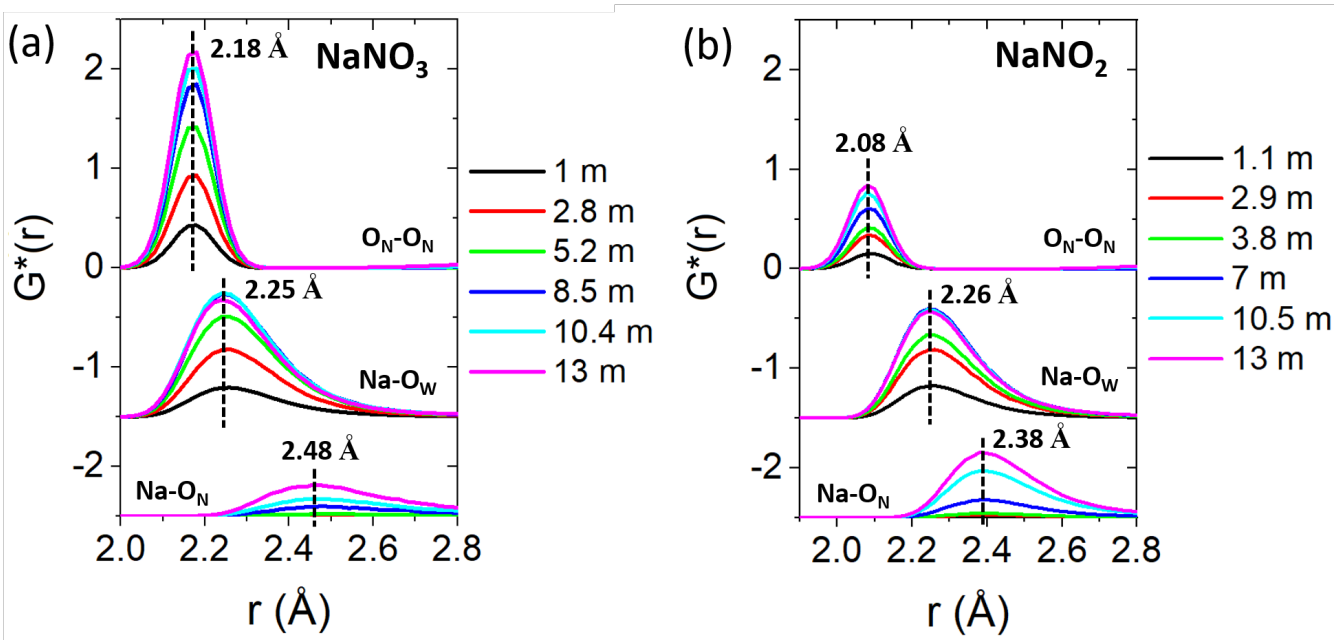

Figure S4: Simulated pair-wise PDF contributions to feature **B** observed in the PDF of $NaNO_{3(aq)}$ and $NaNO_{2(aq)}$ as a function of electrolyte concentration. $G^*(r)$ is the partial X-ray weighted PDF and is calculated using Eqn. S4. Na-O_W and Na-O_N $G^*(r)$ are translated in the y-direction by -1.5 and -2.5 respectively to help guide the eye.

Table S5: Percentage observations of coordination environment of Na^+ in $NaNO_2$ and $NaNO_3$ solutions from CMD. Numbers are in %. Rare cases are not listed here.

$NaNO_{2(aq)}$									
Coordination types	1.1 m	1.9 m	2.9 m	3.8 m	6 m	7 m	9.3 m	10.5 m	13 m
($5H_2O$, $0NO_2^-$)	36.6	31.1	31.1	26.1	22.7	17.4	13.5	9.1	7.5
($6H_2O$, $0NO_2^-$)	55.2	58.4	51.5	52.5	42	35.6	23.8	22.4	15.4
($3H_2O$, $1NO_2^-$)	1.4	1.2	2.5	2.4	3.8	3.8	4.2	2.5	2.4
($4H_2O$, $1NO_2^-$)	3.5	4.3	7.5	8.9	13.3	14.7	15.2	11.6	10
($5H_2O$, $1NO_2^-$)	2.1	3.4	4.9	6.7	9.7	12.6	12.1	12.7	10.2
($2H_2O$, $2NO_2^-$)	0.1	0.1	0.6	0.9	2.5	3.7	6	4.1	3.9
($3H_2O$, $2NO_2^-$)	0.1	0.1	0.5	0.9	2.9	5	8.8	7.8	7.8
($4H_2O$, $2NO_2^-$)	0	0	0.2	0.4	1.2	2.6	4.6	5.6	5.5
($1H_2O$, $3NO_2^-$)	0	0	0	0	0.4	0.9	2.7	2.5	3.4
($2H_2O$, $3NO_2^-$)	0	0	0	0	0.2	1	3.6	4.2	6.5
($3H_2O$, $3NO_2^-$)	0	0	0	0	0.1	0.4	1.8	2.8	4.4
($0H_2O$, $4NO_2^-$)	0	0	0	0	0.1	0.1	0.7	1.4	2.8
($1H_2O$, $4NO_2^-$)	0	0	0	0	0	0.2	1	2.7	5.5
($2H_2O$, $4NO_2^-$)	0	0	0	0	0	0.1	0.5	2.3	3.4
($0H_2O$, $5NO_2^-$)	0	0	0	0	0	0	0.2	1.5	3.8
($1H_2O$, $5NO_2^-$)	0	0	0	0	0	0	0.1	1.8	3.6
($0H_2O$, $6NO_2^-$)	0	0	0	0	0	0	0.1	2.4	2.2

$NaNO_{3(aq)}$						
Coordination types	1 m	2.8 m	5.2 m	8.5 m	10.4 m	13 m
($5H_2O$, $0NO_3^-$)	38.2	35.9	26.5	21.1	15.6	8.6
($6H_2O$, $0NO_3^-$)	57.9	54.9	51.6	34.3	24.9	17.7
($4H_2O$, $1NO_3^-$)	0.8	2.6	5	11	12.1	9.3
($5H_2O$, $1NO_3^-$)	1.8	5	12	18.6	19.6	18.8
($3H_2O$, $2NO_3^-$)	0	0.2	0.7	4.1	7	7.5
($4H_2O$, $2NO_3^-$)	0	0.2	1.2	5.4	9	12.4
($2H_2O$, $3NO_3^-$)	0	0	0.1	1.3	3.2	5.2
($3H_2O$, $3NO_3^-$)	0	0	0.1	1.2	3	6.6
($1H_2O$, $4NO_3^-$)	0	0	0	0.3	1.3	3.3
($2H_2O$, $4NO_3^-$)	0	0	0	0.2	0.9	3.2
($0H_2O$, $5NO_3^-$)	0	0	0	0.1	0.3	1.4
($1H_2O$, $5NO_3^-$)	0	0	0	0	0.2	1.2

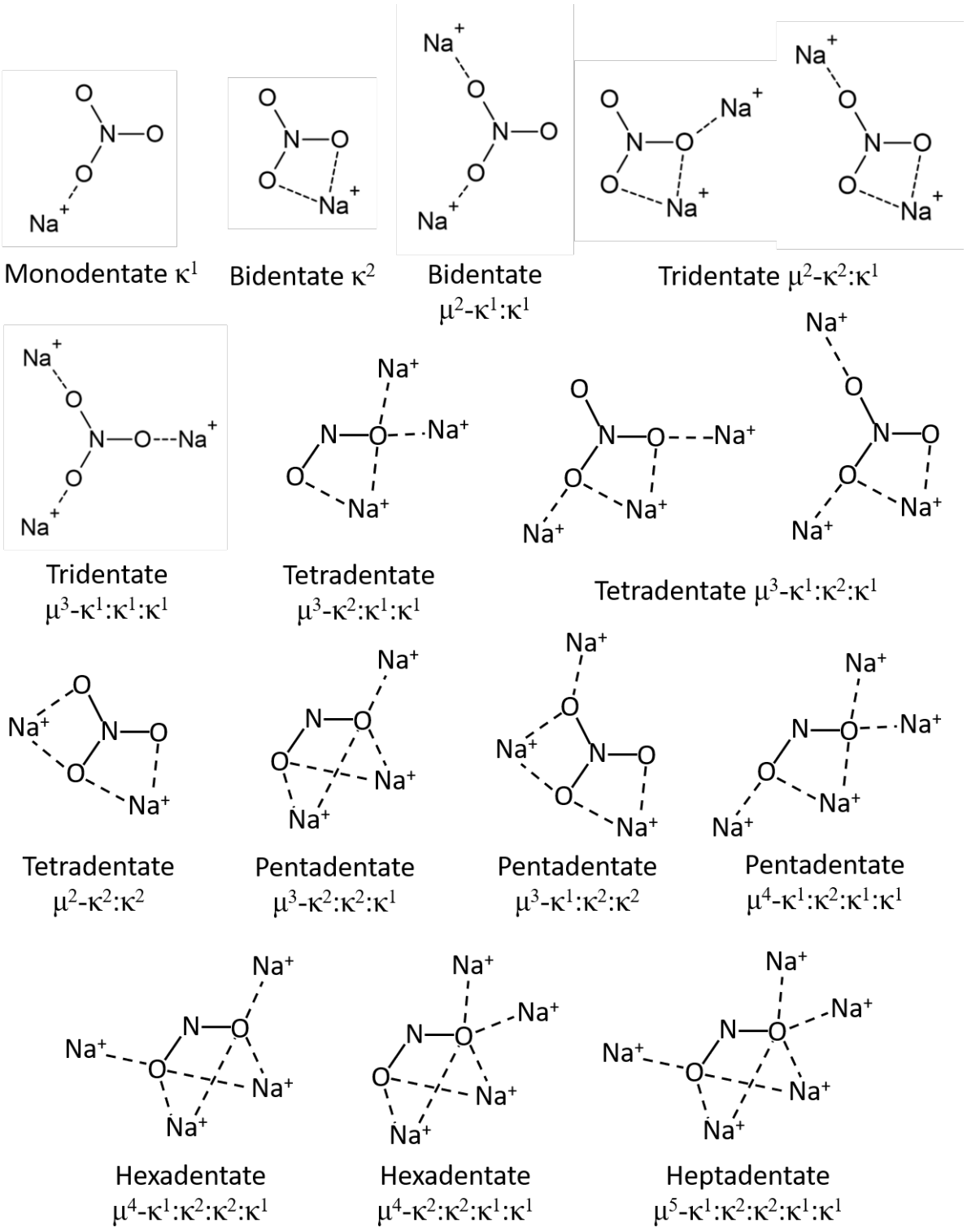

Figure S5: Nomenclature of NO_3^- and NO_2^- denticity referenced from Ref. 37

Table S6: Percentage observations of free cation and anion binding modes in $NaNO_{3(aq)}$ and $NaNO_{2(aq)}$ solutions from CMD. Numbers are in %. Rare cases of anion binding modes are not listed here.

$NaNO_2$ concentration (m)		1.1	1.9	2.9	3.8	6	7	9.3	10.5	13
Free cation		50.4	31.7	12.2	6	1.1	0.6	0.1	0.3	0.2
Non-binding	Free anion	41.7	24.7	11.3	5.3	0.9	0.3	0.1	0.2	0.2
	SSIP anion	51	66.3	71.9	74.2	63.5	53	35	30.8	21.2
Monodentate κ^1		3.2	4	6.6	8.2	12.5	13.1	12.8	11.1	8.4
Bidentate κ^2		4.1	4.6	9	10.3	16.6	19.9	20.7	17.9	15
Tridentate μ_2-κ^2:κ^1		0.1	0.3	0.7	1.3	4.1	7.7	14	13.2	13.5
Tetradentate μ_3-κ^2:κ^1:κ^1		0	0	0	0	0.2	0.6	2.3	2.9	5
Tetradentate μ_3-κ^1:κ^2:κ^1		0	0	0	0	0.2	0.9	2.6	2.8	4.5
Tetradentate μ_2-κ^2:κ^2		0	0	0.1	0.2	0.6	1.5	2.6	2.7	2.8
Pentadentate μ_3-κ^2:κ^2:κ^1		0	0	0	0	0.2	0.8	2.2	3.4	5.2
Pentadentate μ_4-κ^1:κ^2:κ^1:κ^1		0	0	0	0	0	0.1	1.1	2.3	5.6
Hexadentate μ_4-κ^1:κ^2:κ^2:κ^1		0	0	0	0	0	0.1	0.7	1.7	3.3
Hexadentate μ_4-κ^2:κ^2:κ^1:κ^1		0	0	0	0	0	0	0.2	1.4	2.7
Heptadentate μ_5-κ^1:κ^2:κ^2:κ^1:κ^1		0	0	0	0	0	0	0.1	1.6	3.2

$NaNO_3$ concentration (m)		1	2.8	5.2	8.5	10.4	13
Free cation		72	28.9	6.2	0.9	0.3	0.1
Non-binding	Free anion	59.7	23.5	5.7	0.4	0.2	0.1
	SSIP anion	37.7	68.3	74	52.9	35.1	18.9
Monodentate κ^1		2.3	6.9	14.6	25.4	26.9	21
Bidentate κ^2		0.3	1.1	4	9.5	12.4	13
Bidentate μ_2-κ^1:κ^1		0	0.2	0.9	4.5	7.6	9.2
Tridentate μ_2-κ^2:κ^1 (left)		0	0	0.3	2.4	5.5	10
Tridentate μ_2-κ^2:κ^1 (right)		0	0	0.2	1.8	3.5	5.1
Tridentate μ_3-κ^1:κ^1:κ^1		0	0	0	0.3	0.8	1.6
Tetradentate μ_2-κ^2:κ^2		0	0	0.1	0.7	1.6	3.1
Tetradentate μ_3-κ^1:κ^2:κ^1 (left)		0	0	0	0.2	0.7	1.7
Tetradentate μ_3-κ^1:κ^2:κ^1 (right)		0	0	0	0.6	1.9	5.1
Pentadentate μ_3-κ^1:κ^2:κ^2		0	0	0	0.2	0.7	2.3

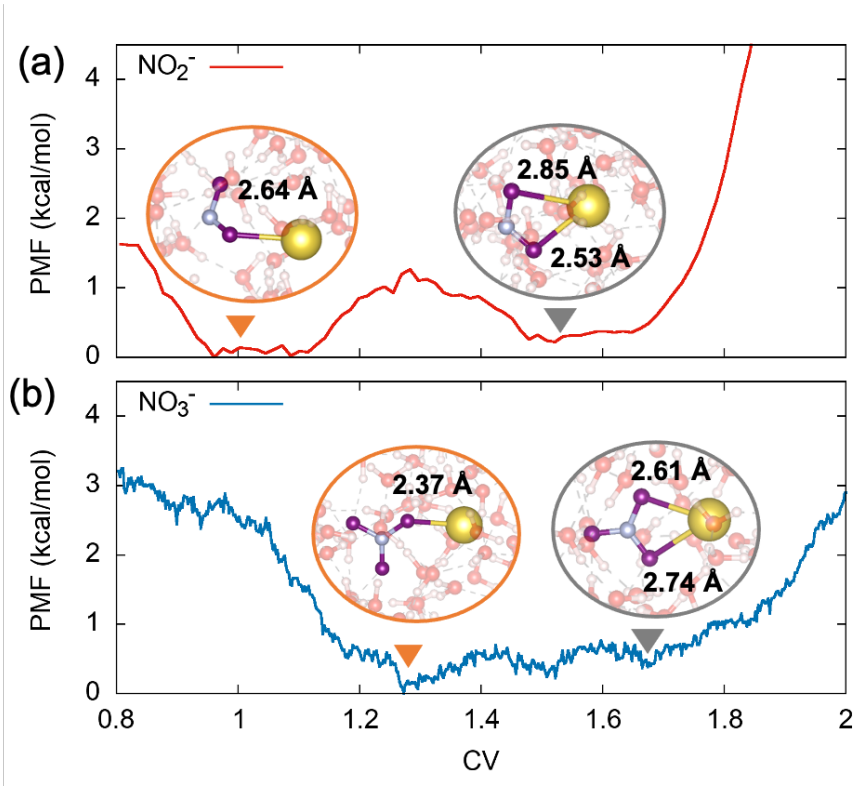

Figure S6: Ab initio molecular dynamics potential of mean force mapping the energy change between bidentate and monodentate coordination of NO_3^- and NO_2^- to Na^+ in bulk water. Snapshots at specific CV values and the corresponding On-Na distance plotted as insets. Two distinct minima are observed for mono- and bidentate coordination of NO_2^- to Na^+ with a small barrier for interconversion. For NO_3^-, a more broad minima is observed that favors the monodentate coordination with little stabilization of the bidentate coordination environment. This is consistent with the trends in denticity in the bulk electrolyte CMD simulations.

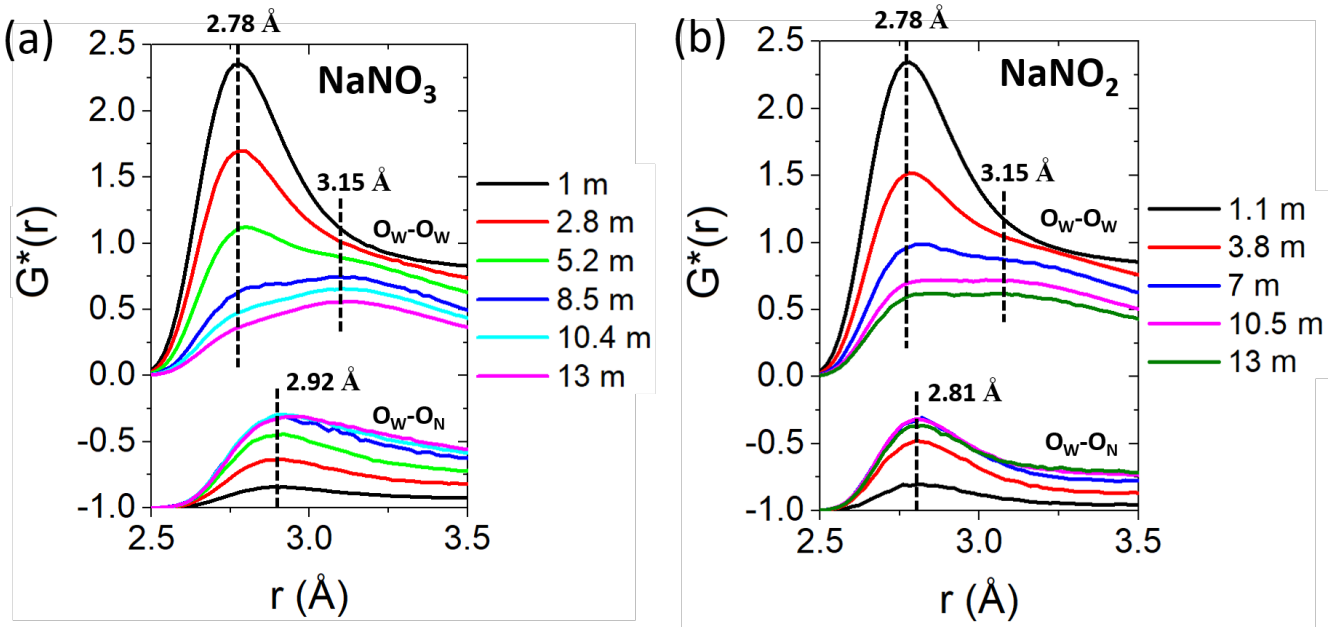

Figure S7: Simulated pair-wise PDF contributions to features **C** – **D** in the PDF of $NaNO_{3(aq)}$ and $NaNO_{2(aq)}$ as a function of electrolyte concentration. $G^*(r)$ is calculated using Eqn. S4. O_W-O_N $G^*(r)$ is translated in y-direction by -1 for better comparison.

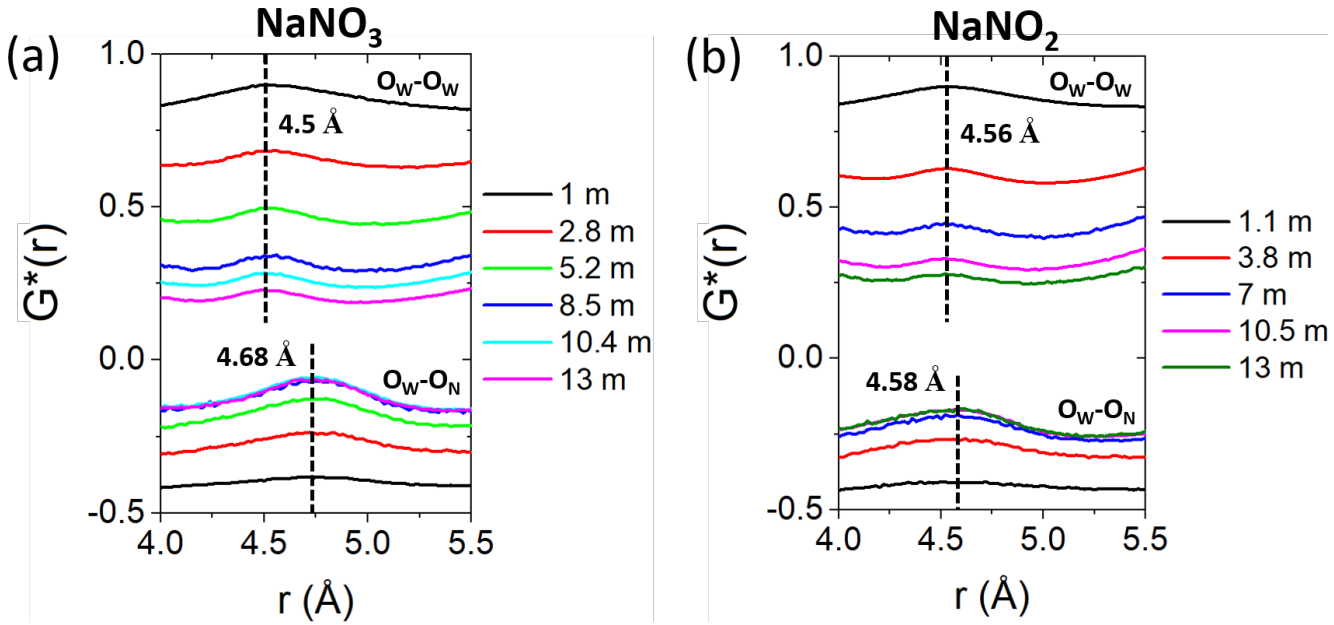

Figure S8: Simulated pair-wise PDF contributions to feature **E** in the PDF of $NaNO_{3(aq)}$ and $NaNO_{2(aq)}$ as a function of electrolyte concentration. $G^*(r)$ is calculated using Eqn. S4. O_W-O_N $G^*(r)$ is translated in y-direction by -0.5 for better comparison.

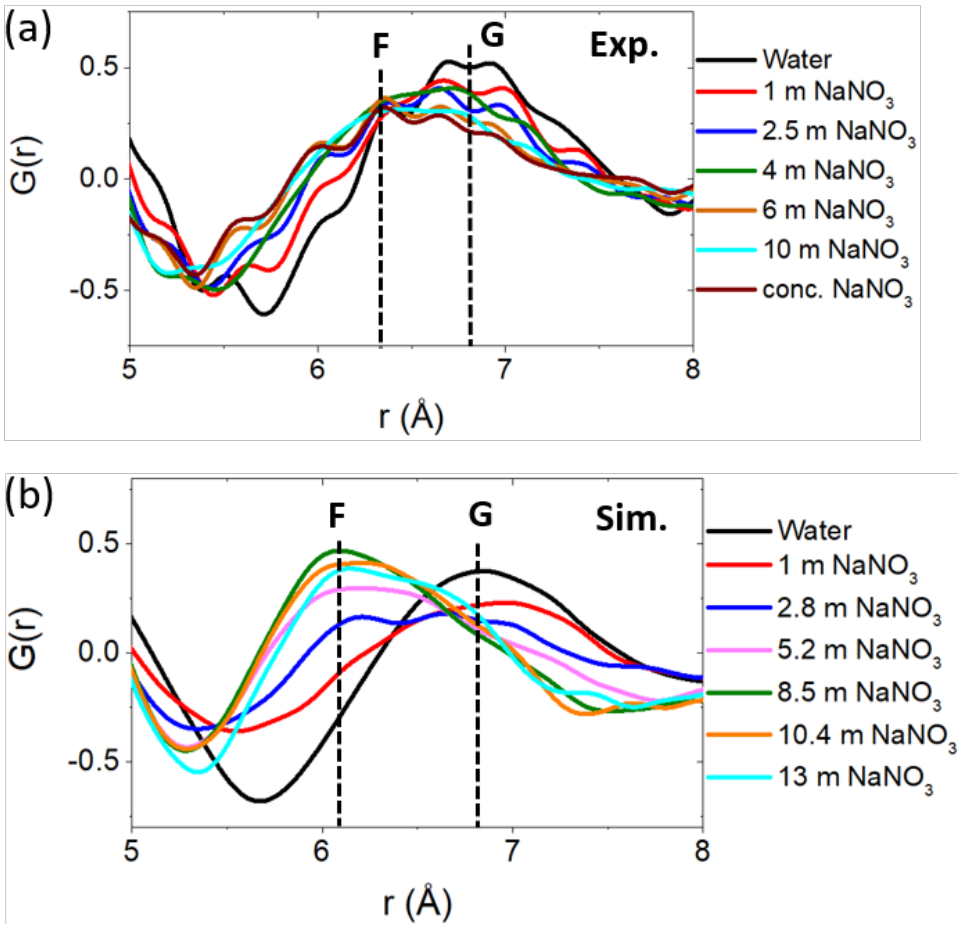

Figure S9: Long-range experimental (a) and simulated (b) total X-ray PDFs for $NaNO_{3(aq)}$. Simulated $G(r)$ is calculated using DISCUS.[13]

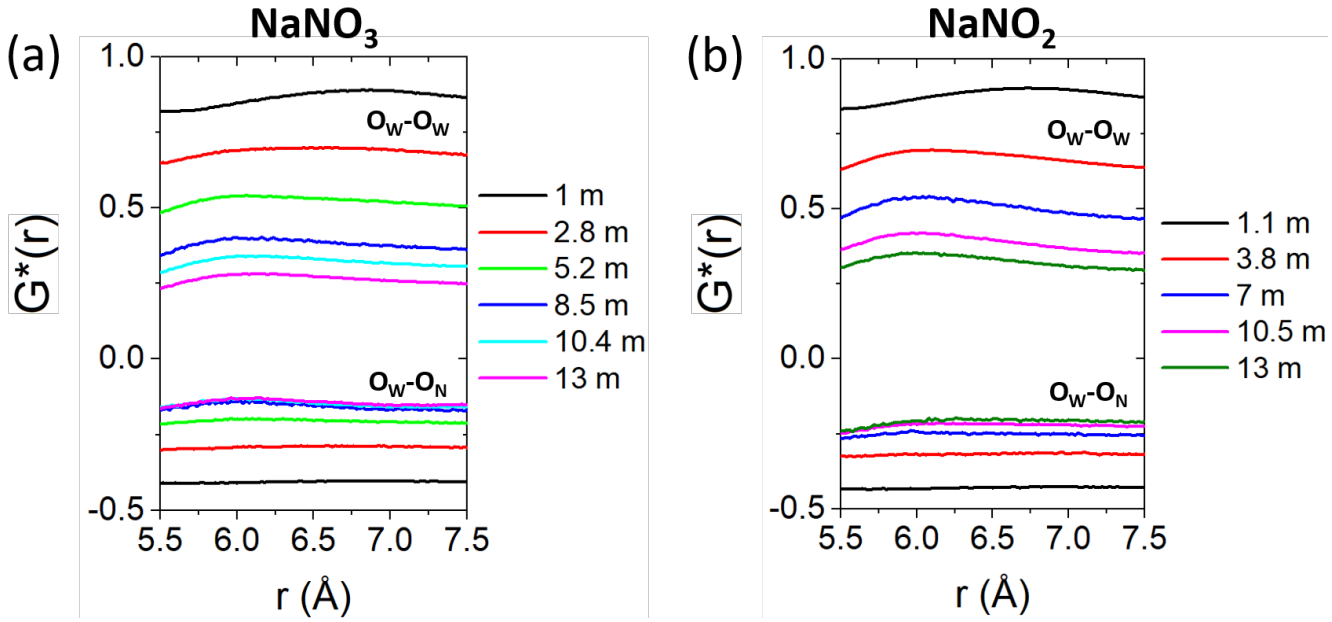

Figure S10: Simulated pair-wise PDF contributions to feature **F** – **G** in the PDF of $NaNO_{3(aq)}$ and $NaNO_{2(aq)}$ as a function of electrolyte concentration. $G^*(r)$ is calculated using Eqn. S4. O_W-O_N $G^*(r)$ is translated in y-direction by -0.5 for better comparison.

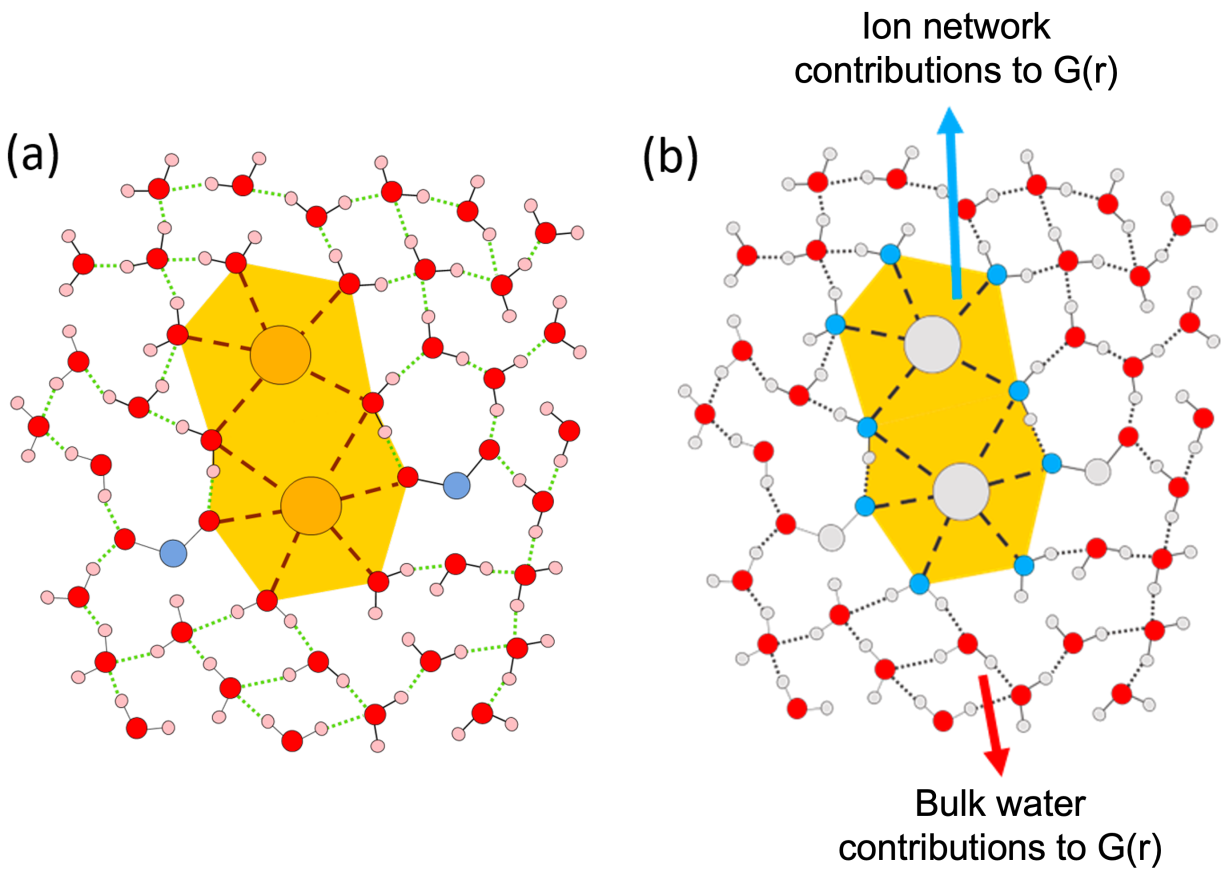

Figure S11: (a) Schematic image of $NaNO_2$ aqueous electrolyte system. Circles with colors represent different atom types: oxygen (red), hydrogen (pink), sodium (orange), nitrogen (cyan). Dashed lines represent intermolecular interactions. (b) An illustration of partitioning of the atom-pair correlations into two networks, those in red are associated with H_2O that are not part of the Na^+ solvation shell or coordination shell polyhedra, while those in blue are all O-atoms that directly coordinate Na^+.

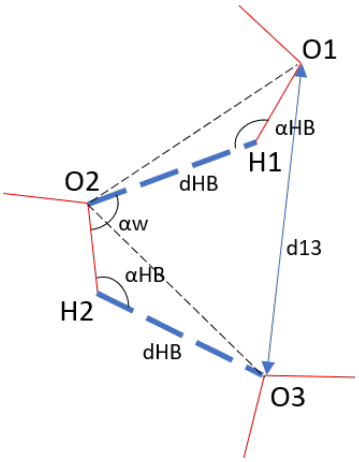

Figure S12: Geometric model of HB variations.

Table S7: Modeled changes in the 3-water O1$\cdots$O3 distance as a function of hydrogen bond distance and angles (labelling shown in Figure S12).

d_{HB} (Å)	α_{HB} (°)	$d_{O1\cdots O2}$ (Å)	$d_{O1\cdots O3}$ (Å)
1.6	140	2.45	3.75
1.6	150	2.52	3.92
1.6	160	2.56	4.06
1.7	140	2.56	3.87
1.7	150	2.61	4.05
1.7	160	2.66	4.20
1.8	140	2.64	3.98
1.8	150	2.71	4.18
1.8	160	2.76	4.34
1.9	140	2.74	4.09
1.9	150	2.81	4.30
1.9	160	2.86	4.48

Table S8: Observed oligomer probability from CMD as a function of electrolyte concentration. Oligomers with observation probability less than 1% are not listed.

$NaNO_{3(aq)}$				
Concentration (m)	% dimer	% trimer	% tetramer	% pentamer
1.0	99	1	0	0
2.8	98	2	0	0
5.2	89	10	1	0
8.5	68	18	7	3
10.4	54	18	9	5
13.0	50	16	8	5
$NaNO_{2(aq)}$				
Concentration (m)	% dimer	% trimer	% tetramer	% pentamer
1.1	99	1	0	0
1.9	96	3	0	0
2.9	94	6	0	0
3.8	89	10	1	0
6.0	79	15	4	1
7.0	65	20	8	4
9.3	51	20	10	6
10.5	51	19	9	5
13.0	50	17	8	4

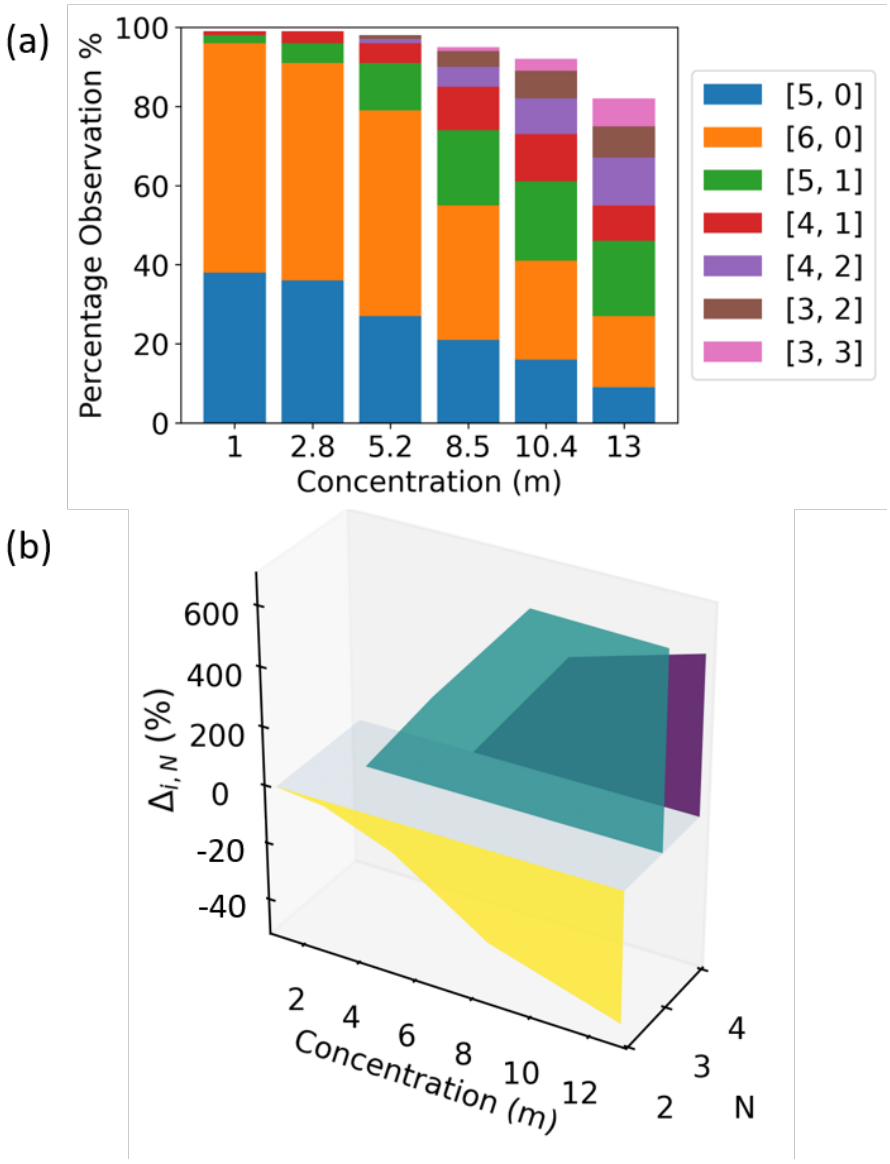

Figure S13: (a) Percent observation of coordination environment of Na^+ as a function of [$NaNO_3$] from CMD. Labels [a, b] indicates number of coordinated H_2O and NO_3^-. Number distribution provided in Table S7. Only the top seven coordination environments are plotted here. (b) The % change $\Delta_{i,N}$ of Na^+ coordination polyhedron and their oligomers of size N as a function [$NaNO_3$] from CMD. $\Delta_{i,N} = (P_{i,N} - P_{c,N})/P_{c,N}$, where P is the probability of observation at at a concentration i relative to the lowest concentration c for which N-oligomer size is observed. The decrease in observation of $N = 3$ and 4 at high [$NaNO_2$] is attributed to highly fluxional large N that occur at low frequency and are not reported. Number distribution provided in Table S8.

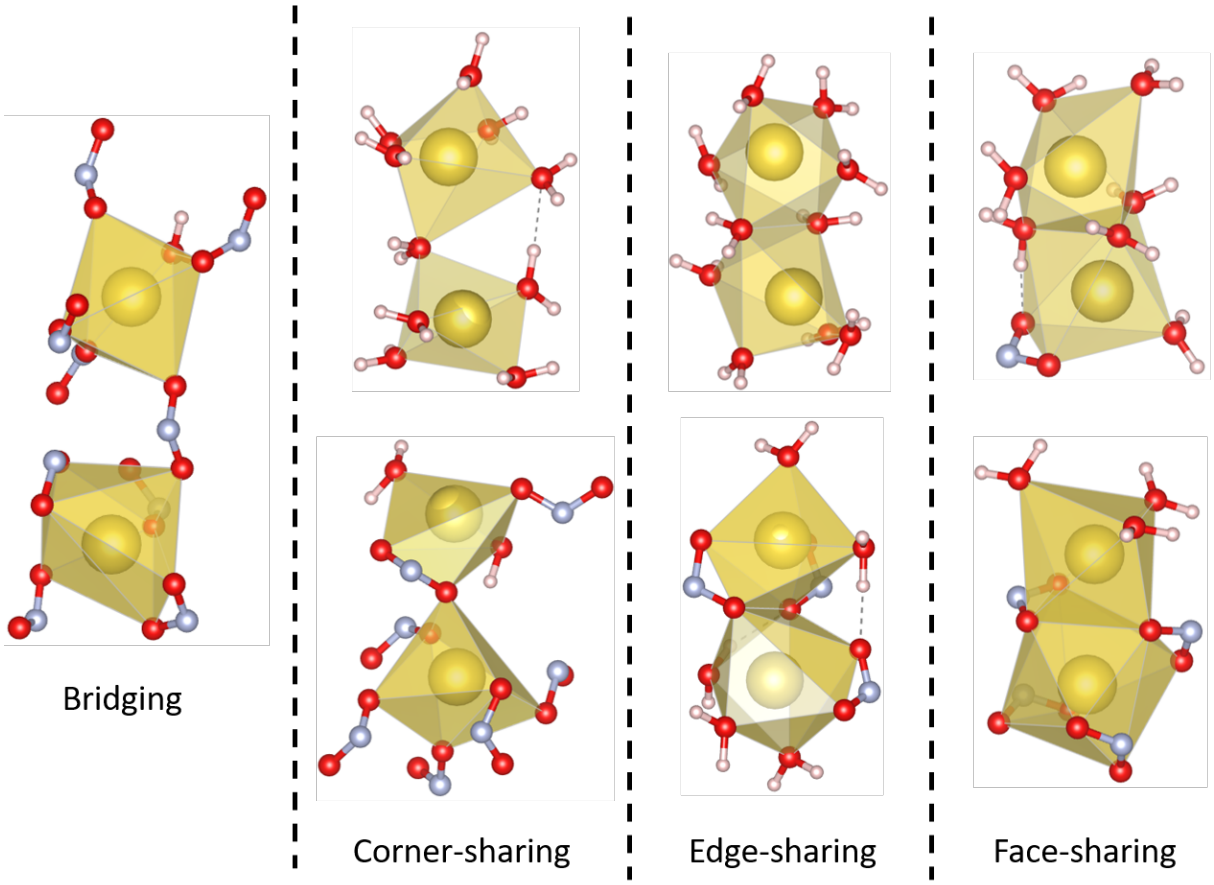

Figure S14: Examples of polyhedra linking types in $NaNO_2$ solutions.

Table S9: Observed polyhedron linking types from CMD as a function of electrolyte concentration.

$NaNO_{3(aq)}$				
Concentration (m)	% Bridging	% Corner-sharing	% Edge-sharing	% Face-sharing
1.0	1	23	15	4
2.8	4	47	33	7
5.2	9	48	33	10
8.5	24	40	28	8
10.4	34	36	23	7
13.0	37	30	17	6
$NaNO_{2(aq)}$				
Concentration (m)	% Bridging	% Corner-sharing	% Edge-sharing	% Face-sharing
1.1	0	17	13	3
1.9	0	39	22	8
2.9	2	51	35	10
3.8	2	54	34	10
6.0	4	52	34	10
7.0	6	50	31	13
9.3	11	45	29	13
10.5	20	35	23	19
13.0	21	33	23	19

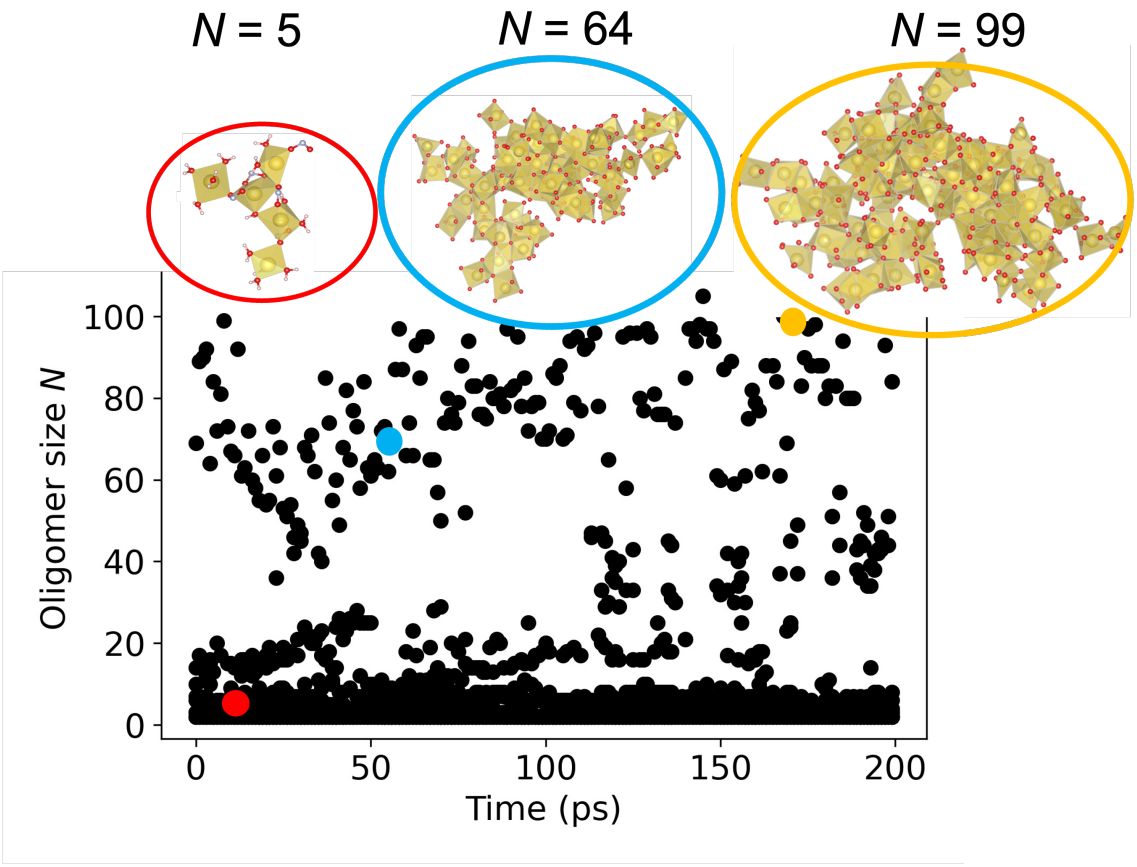

Figure S15: Change in oligomer size in $NaNO_{3(aq)}$ over time.

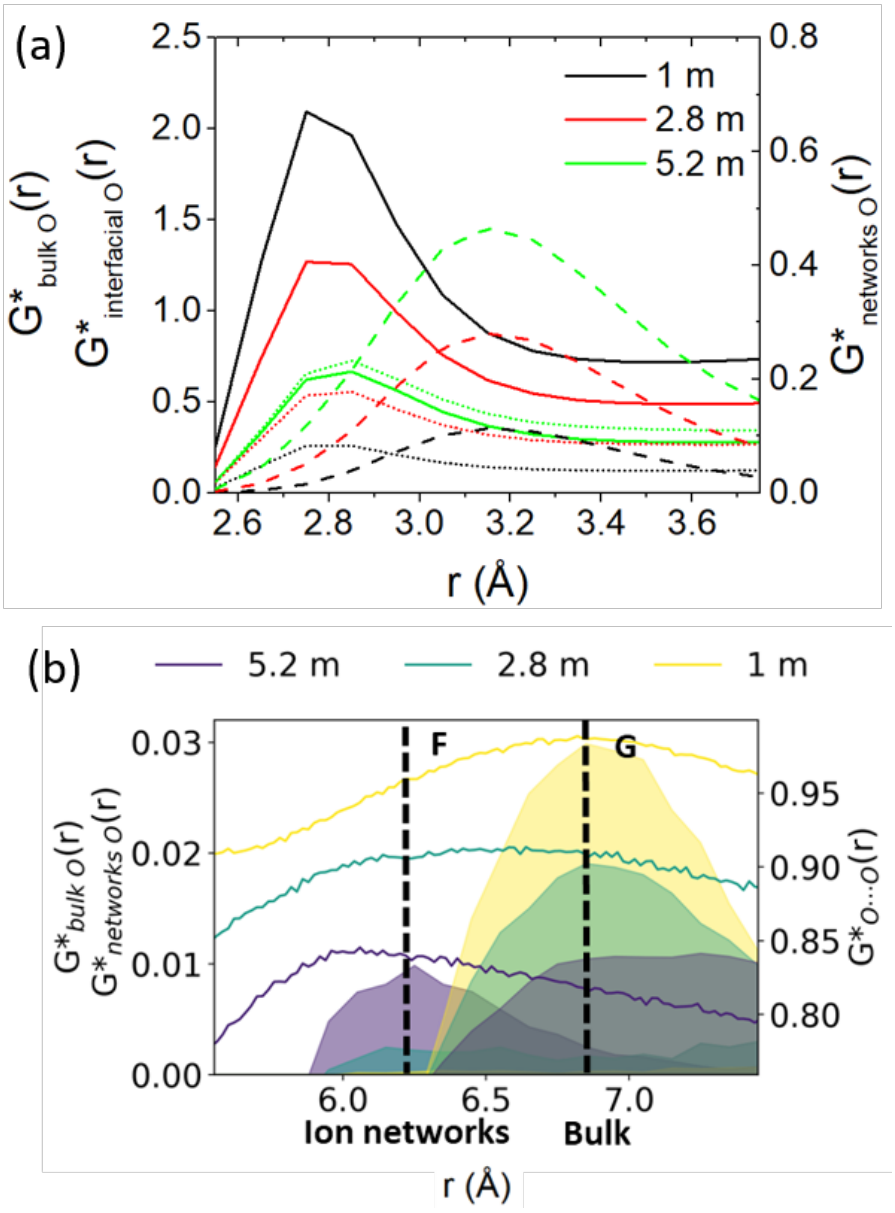

Figure S16: (a) Simulated partial XRD PDFs of different oxygen states in $NaNO_3$ solutions at mid-range. Solid lines: bulk O $\cdots$ O; dash lines: networks O $\cdots$ O; dot lines: interfacial O $\cdots$ O. (b) Simulated partial XRD PDFs of O$\cdots$O (solid lines) and different oxygen states (shaded lines, calculated using Eqn. S4) in $NaNO_3$ solutions at long-range. $G^*(r)$ of bulk O and networks O are aligned by moving the averaged $G^*(r)$ from 5.5-7.5 Å to 0.

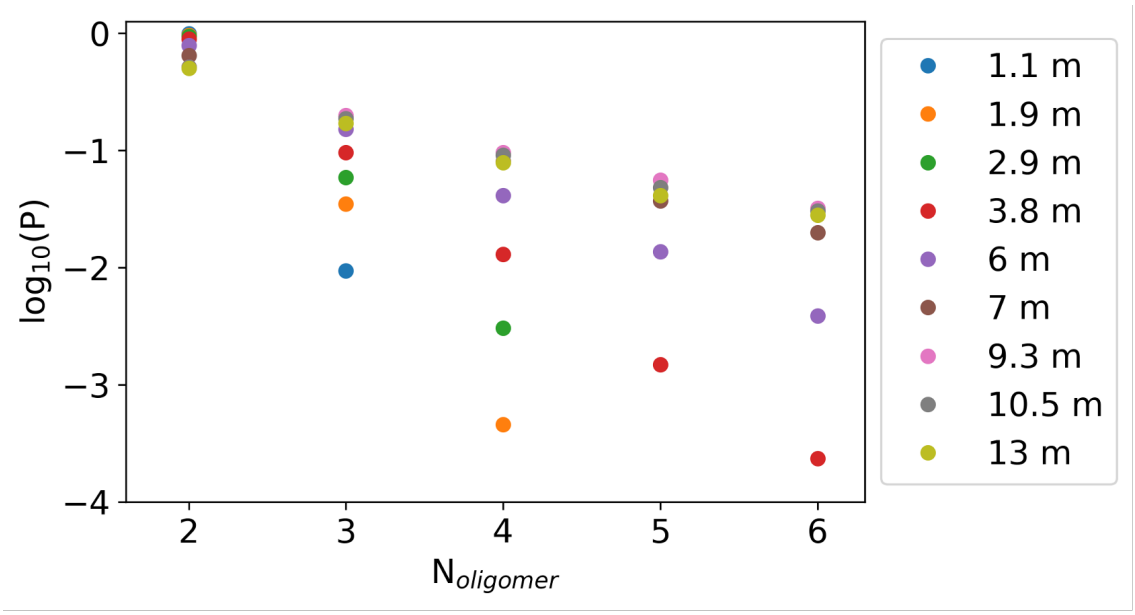

Figure S17: Log plot of oligomer size distribution as a function of concentration for $NaNO_{3(aq)}$.

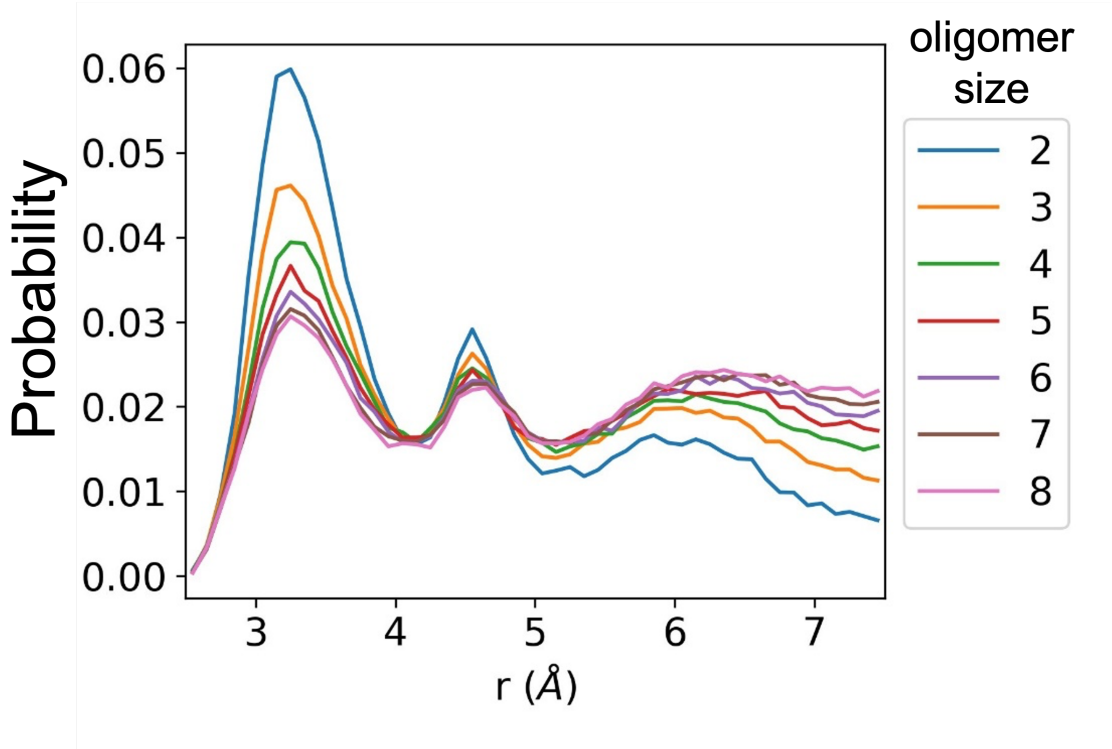

Figure S18: Probability of observation of different O...O distances in each oligomer up to the 8-mer in $NaNO_{3(aq)}$ over all concentrations.

References

(1) Toby, B. H.; Von Dreele, R. B. GSAS-II: the genesis of a modern open-source all purpose crystallography software package. *Journal of Applied Crystallography* **2013**, *46*, 544–549.

(2) Qiu, X.; Thompson, J. W.; Billinge, S. J. PDFgetX2: a GUI-driven program to obtain the pair distribution function from X-ray powder diffraction data. *Journal of Applied Crystallography* **2004**, *37*, 678–678.

(3) Van Der Spoel, D.; Lindahl, E.; Hess, B.; Groenhof, G.; Mark, A. E.; Berendsen, H. J. GROMACS: fast, flexible, and free. *Journal of Computational Chemistry* **2005**, *26*, 1701–1718.

(4) Martínez, L.; Andrade, R.; Birgin, E. G.; Martínez, J. M. PACKMOL: A package for building initial configurations for molecular dynamics simulations. *Journal of Computational Chemistry* **2009**, *30*, 2157–2164.

(5) Nosé, S. A molecular dynamics method for simulations in the canonical ensemble. *Mol. Phys.* **1984**, *52*, 255–268.

(6) Hoover, W. G. Canonical dynamics: Equilibrium phase-space distributions. *Phys. Rev. A* **1985**, *31*, 1695.

(7) Parrinello, M.; Rahman, A. Polymorphic transitions in single crystals: A new molecular dynamics method. *J. Appl. Phys.* **1981**, *52*, 7182–7190.

(8) Darden, T.; York, D.; Pedersen, L. Particle mesh Ewald: An N log (N) method for Ewald sums in large systems. *The Journal of Chemical Physics* **1993**, *98*, 10089–10092.

(9) Berendsen, H. J.; Postma, J. P.; van Gunsteren, W. F.; Hermans, J. Interaction models for water in relation to protein hydration. Intermolecular forces: proceedings of

the fourteenth Jerusalem symposium on quantum chemistry and biochemistry held in Jerusalem, Israel, April 13–16, 1981. 1981; pp 331–342.

(10) Hess, B.; Bekker, H.; Berendsen, H. J.; Fraaije, J. G. LINCS: A linear constraint solver for molecular simulations. *Journal of Computational Chemistry* **1997**, *18*, 1463–1472.

(11) Oostenbrink, C.; Villa, A.; Mark, A. E.; Van Gunsteren, W. F. A biomolecular force field based on the free enthalpy of hydration and solvation: the GROMOS force-field parameter sets 53A5 and 53A6. *Journal of Computational Chemistry* **2004**, *25*, 1656–1676.

(12) Cordeiro, R. M.; Yusupov, M.; Razzokov, J.; Bogaerts, A. Parametrization and molecular dynamics simulations of nitrogen oxyanions and oxyacids for applications in atmospheric and biomolecular sciences. *The Journal of Physical Chemistry B* **2020**, *124*, 1082–1089.

(13) Proffen, T.; Neder, R. B. *DISCUS*: a program for diffuse scattering and defect-structure simulation. *J. Appl. Cryst.* **1997**, *30*, 171–175.

(14) Prange, M. P.; Mergelsberg, S. T.; Kerisit, S. N. Ab initio molecular dynamics simulations of amorphous calcium carbonate: Interpretation of pair distribution function and X-ray absorption spectroscopy data. *Crystal Growth & Design* **2021**, *21*, 2212–2221.

(15) Prange, M. P.; Mergelsberg, S. T.; Kerisit, S. N. Structural water in amorphous carbonate minerals: ab initio molecular dynamics simulations of X-ray pair distribution experiments. *Physical Chemistry Chemical Physics* **2023**, *25*, 6768–6779.

(16) Kerisit, S. N.; Prange, M. P.; Mergelsberg, S. T. Local density changes and carbonate rotation enable Ba incorporation in amorphous calcium carbonate. *Chemical Communications* **2023**, *59*, 6379–6382.

(17) Megyes, T., et al. Solution structure of NaNO3 in water: Diffraction and molecular dynamics simulation study. *The Journal of Physical Chemistry B* **2009**, *113*, 4054–4064.

(18) Guilbaud, P.; Wipff, G. Hydration of uranyl (UO22+) cation and its nitrate ion and 18-crown-6 adducts studied by molecular dynamics simulations. *J. Phys. Chem.* **1993**, *97*, 5685–5692.

(19) Zou, J. A Kirkwood-Buff Force Field for polyoxoanions in water. Ph.D. thesis, Kansas State University, 2010.

(20) Kam, H. C.; Ranathunga, D. T.; Payne, E. R.; Smaldone, R. A.; Nielsen, S. O.; Dodani, S. C. Spectroscopic characterization and in silico modelling of polyvinylpyrrolidone as an anion-responsive fluorescent polymer in aqueous media. *Supramolecular Chemistry* **2019**, *31*, 514–522.

(21) Richards, L. A.; Schäfer, A. I.; Richards, B. S.; Corry, B. The importance of dehydration in determining ion transport in narrow pores. *Small* **2012**, *8*, 1701–1709.

(22) Berendsen, H. J.; Grigera, J. R.; Straatsma, T. P. The missing term in effective pair potentials. *Journal of Physical Chemistry* **1987**, *91*, 6269–6271.

(23) Jorgensen, W. L.; Maxwell, D. S.; Tirado-Rives, J. Development and testing of the OPLS all-atom force field on conformational energetics and properties of organic liquids. *Journal of the American Chemical Society* **1996**, *118*, 11225–11236.

(24) Jorgensen, e. a., William L. Comparison of simple potential functions for simulating liquid water. *J. Chem. Phys.* **1983**, *79*, 926–935.

(25) Vanommeslaeghe, K.; Hatcher, E.; Acharya, C.; Kundu, S.; Zhong, S.; Shim, J.; Darian, E.; Guvench, O.; Lopes, P.; Vorobyov, I., et al. CHARMM general force field: A

force field for drug-like molecules compatible with the CHARMM all-atom additive biological force fields. *Journal of Computational Chemistry* **2010**, *31*, 671–690.

(26) Wang, J.; Wolf, R. M.; Caldwell, J. W.; Kollman, P. A.; Case, D. A. Development and testing of a general amber force field. *Journal of Computational Chemistry* **2004**, *25*, 1157–1174.

(27) Joung, I. S.; Cheatham III, T. E. Determination of alkali and halide monovalent ion parameters for use in explicitly solvated biomolecular simulations. *J. Phys. Chem. B* **2008**, *112*, 9020–9041.

(28) Vchirawongkwin, S.; Kritayakornupong, C.; Tongraar, A.; Vchirawongkwin, V. Hydration properties determining the reactivity of nitrite in aqueous solution. *Dalton Transactions* **2014**, *43*, 12164–12174.

(29) Vchirawongkwin, V.; Kritayakornupong, C.; Tongraar, A.; Rode, B. M. Symmetry breaking and hydration structure of carbonate and nitrate in aqueous solutions: A study by ab initio quantum mechanical charge field molecular dynamics. *The Journal of Physical Chemistry B* **2011**, *115*, 12527–12536.

(30) Kresse, G.; Hafner, J. Ab initio molecular dynamics for liquid metals. *Phys. Rev. B* **1993**, *47*, 558.

(31) Kresse, G.; Furthmüller, J. Efficient iterative schemes for ab initio total-energy calculations using a plane-wave basis set. *Phys. Rev. B* **1996**, *54*, 11169.

(32) Perdew, J. P.; Burke, K.; Ernzerhof, M. Generalized gradient approximation made simple. *Physical Review Letters* **1996**, *77*, 3865.

(33) Kresse, G.; Joubert, D. From ultrasoft pseudopotentials to the projector augmented-wave method. *Phys. Rev. B* **1999**, *59*, 1758.

(34) Grossfield, A. WHAM: the weighted histogram analysis method. 2003; `http://membrane.urmc.rochester.edu/wordpress/?page_id=126`.

(35) Hudelson, M.; Mooney, B. L.; Clark, A. E. Determining polyhedral arrangements of atoms using PageRank. *Journal of Mathematical Chemistry* **2012**, *50*, 2342–2350.

(36) Brin, S.; Page, L. The Anatomy of a Large-Scale Hypertextual Web Search Engine. Proceedings of the Seventh International Conference on World Wide Web 7. NLD, 1998; p 107–117.

(37) Saxena, P.; Thirupathi, N. Reactions of Cd (OAc) 2· 2H2O with variously substituted pyridines. Efforts to unravel the factors that determine structure/nuclearity of the products. *Polyhedron* **2015**, *98*, 238–250.